



 Cite this: *RSC Adv.*, 2020, **10**, 33628

 Received 7th July 2020
 Accepted 24th August 2020

DOI: 10.1039/d0ra05926a

rsc.li/rsc-advances

Two 3D Mn-based coordination polymers: synthesis, structure and magnetocaloric effect†

 Ning-Fang Li, Ye-Min Han, Jia-Nian Li, Jia-Peng Cao, Ze-Yu Du and Yan Xu *

Two three-dimensional (3D) coordination polymers, namely $\text{Mn}_6^{\text{II}}(\text{CH}_3\text{COO})_2(\text{HCOO})_2(\text{IN})_8(\text{C}_4\text{H}_8\text{O})_2(\text{H}_2\text{O})$ and $\text{Mn}_6^{\text{III}}\text{Mn}_{12}^{\text{II}}(\mu_3\text{-O})_6(\text{CH}_3\text{COO})_{12}(\text{IN})_{18}(\text{H}_2\text{O})_{7.5}$ (abbreviated as Mn_6^{II} and $\text{Mn}_{12}^{\text{II}}\text{Mn}_6^{\text{III}}$ respectively; HIN = isonicotinic acid), were synthesized by the reaction of $\text{Mn}(\text{CH}_3\text{COO})_2 \cdot 4\text{H}_2\text{O}$ and isonicotinic acid under solvothermal conditions. Magnetic studies revealed that antiferromagnetic interactions may be present in compounds Mn_6^{II} and $\text{Mn}_{12}^{\text{II}}\text{Mn}_6^{\text{III}}$. Moreover, the values of $-\Delta S_{\text{m}}$ (26.27 (Mn_6^{II}) and 37.69 ($\text{Mn}_{12}^{\text{II}}\text{Mn}_6^{\text{III}}$) $\text{J kg}^{-1} \text{K}^{-1}$ at $\Delta H = 7$ T) are relatively larger than those of the reported Mn-based coordination polymers. This work provides a great scope in the magnetocaloric effect (MCE) of pure 3d-type systems.

Introduction

Manganese (Mn) ions owing to their variety in valency and coordination numbers make the Mn-based compounds exhibit interesting structures, such as chain-like¹ and wheel-like,^{2,3} as well promising applications in the proton exchange membrane,^{4,5} catalysis,^{6–8} adsorption and so on.^{3,9–15} Moreover, since the discovery of the first case of single-molecule magnet behavior (SMM) in the compound $\text{Mn}_8^{\text{III}}\text{Mn}_4^{\text{IV}}$ in 1980,¹⁶ Mn-based compounds have played an active role in the field of magnetism.^{17–21} For example, Mn_X ($X = 7, 12, 16, 19, 26, 30, 32, 44, 70$, and 84) demonstrate the single-molecule magnet (SMM) behaviour,^{9,17,22–30} and Mn_X ($X = 1, 4, 10, 14$, and 17) demonstrate the magnetocaloric effect (MCE),^{31–34} which can replace expensive and scarce ³He.^{35–40}

Undoubtedly, all molecular magnetic complexes can exhibit MCE to a certain extent.^{35–40} However, only some Gd^{III}-based compounds displayed large magnetic entropy change (ΔS_{m}), which is an important criterion to evaluate MCE.^{37,45–47} Studies manifest that the neglected magnetic anisotropy, large spin ground state (S) and low-lying excited spin states are beneficial to the MCE.^{38,46} Although lanthanide (4f)-type compounds have made a breakthrough in magnetic cooling materials, the search for highly efficient MCE materials without lanthanide remains a crucial issue owing to the expensive and rare 4f compounds.^{41–44} In 2014, $[\text{Mn}(\text{glc})_2(\text{H}_2\text{O})]$ with $\Delta S_{\text{m}} = 60.3 \text{ J kg}^{-1} \text{K}^{-1}$, the value of which is larger than that of the majority of pure Gd-style and 3d-Gd

compounds, was prepared by Tong *et al.*³¹ This example inspires us to study the MCE of 3d-type systems. Thus, we aim at developing a procedure regarding the pure 3d-type systems with MCE.

According to the literature, using HIN as a ligand is a better choice to prepare metal coordination polymers.⁴⁸ The coordination sites (one N- and two O-donors) of HIN can connect at least one metal ion; thus, HIN ligands are beneficial to form high-nuclear metal clusters accompanied with large MCE, such as $\text{Gd}_{52}\text{Ni}_{52}$ with $-\Delta S_{\text{m}} = 35.6 \text{ J kg}^{-1} \text{K}^{-1}$.³⁸

Herein, two six/eighteen-nuclear manganese coordination polymers $\text{Mn}_6^{\text{II}}(\text{CH}_3\text{COO})_2(\text{HCOO})_2(\text{IN})_8(\text{C}_4\text{H}_8\text{O})_2(\text{H}_2\text{O})$ and $\text{Mn}_6^{\text{III}}\text{Mn}_{12}^{\text{II}}(\mu_3\text{-O})_6(\text{CH}_3\text{COO})_{12}(\text{IN})_{18}(\text{H}_2\text{O})_{7.5}$ (abbreviated as Mn_6^{II} and $\text{Mn}_{12}^{\text{II}}\text{Mn}_6^{\text{III}}$, respectively), were successfully obtained by the reaction of $\text{Mn}(\text{CH}_3\text{COO})_2 \cdot 4\text{H}_2\text{O}$ and HIN under solvothermal conditions. The magnetic studies reveal that antiferromagnetic interactions are present in Mn_6^{II} and $\text{Mn}_{12}^{\text{II}}\text{Mn}_6^{\text{III}}$, and both show excellent MCE properties with $-\Delta S_{\text{m}} = 26.27$ (Mn_6^{II}) and 37.69 ($\text{Mn}_{12}^{\text{II}}\text{Mn}_6^{\text{III}}$) $\text{J kg}^{-1} \text{K}^{-1}$. The $-\Delta S_{\text{m}}$ values obtained in this work are relatively larger than those of the existing 3d-based compounds.^{32,33} In 2018, $[\text{Mn}_3^{\text{II}}]_6$, with an interesting wheel structure and 18 metal Mn^{II} ions, was synthesized by Qin *et al.*³ In our study, comparing $\text{Mn}_{12}^{\text{II}}\text{Mn}_6^{\text{III}}$ with $[\text{Mn}_3^{\text{II}}]_6$, we found that (i) the valencies of Mn ions in $\text{Mn}_{12}^{\text{II}}\text{Mn}_6^{\text{III}}$ are +2 and +3, as determined by X-ray photoelectron spectroscopy (XPS); (ii) $[\text{Mn}_3^{\text{II}}]_6$ was mainly applied to sorption; however, we deeply studied the MCE for $\text{Mn}_{12}^{\text{II}}\text{Mn}_6^{\text{III}}$. Moreover, among the current pure Mn-type compounds, $-\Delta S_{\text{m}}$ (37.69 $\text{J kg}^{-1} \text{K}^{-1}$) for $\text{Mn}_{12}^{\text{II}}\text{Mn}_6^{\text{III}}$ is nearly the largest. Our pure Mn-type materials are highly promising applications in MCE.

Experimental section

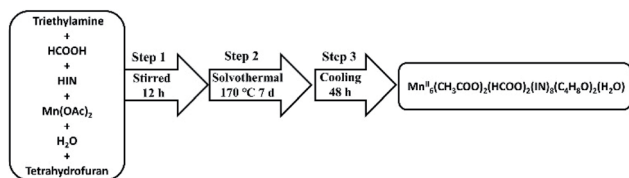
X-ray crystallography

A Bruker Apex II CCD detector was applied to collect the data of single-crystal X-ray diffraction (SCXRD) analyses under 296 K

College of Chemical Engineering, State Key Laboratory of Materials-Oriented Chemical Engineering, Nanjing Tech University, Nanjing 211816, P. R. China. E-mail: yanxu@njtech.edu.cn

† Electronic supplementary information (ESI) available: Physical measurements, crystal synthesis, additional structural pictures, XPS, PXRD, FT-IR spectra, TG analysis, magnetic properties, as well as selected bond lengths and angles. Tables S1, S2, and Fig. S1–S24. CCDC 2004735 and 2004736 for compounds Mn_6^{II} and $\text{Mn}_{12}^{\text{II}}\text{Mn}_6^{\text{III}}$. For ESI and crystallographic data in CIF or other electronic format see DOI: 10.1039/d0ra05926a



Scheme 1 Synthetic route of Mn_6^{II} .

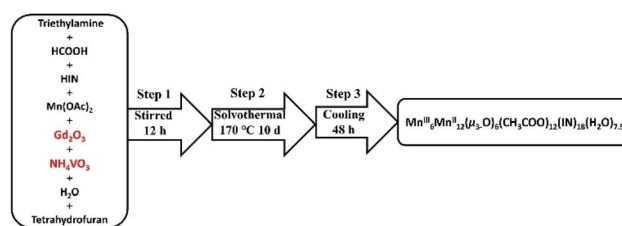
and 50 kV as well 30 mA with a sealed tube X-ray source (Mo-K α radiation, $\lambda = 0.71 \text{ \AA}$). The structures of Mn_6^{II} and $\text{Mn}_{12}^{\text{II}}\text{Mn}_6^{\text{III}}$ were resolved based on direct methods, and were refined based on full-matrix least-squares refinement using the SHELXL-2018/3 program package.

Synthesis of compounds

Preparation of Mn_6^{II} . A mixture of HCOOH (0.023 g 0.50 mmol), ethylenediamine (0.030 g, 0.50 mmol), $\text{Mn} \cdot (\text{CH}_3\text{COO})_2 \cdot 4\text{H}_2\text{O}$ (0.350 g, 2.00 mmol), HIN (0.246 g, 2.0 mmol) and tetrahydrofuran (8.0 mL) was stirred at room temperature for 12 h. Then, this suspension was heated to 170 °C and kept for 7 days in a 25 mL Teflon-lined autoclave (Schemes 1 and S1†). After cooling for 48 h, a colourless block product was obtained. The product was washed with $\text{CH}_3\text{CH}_2\text{OH}$, and the

yield of pure Mn_6^{II} was 68% (based on Mn). Anal. calcd for $\text{C}_{62}\text{H}_{58}\text{Mn}_6\text{N}_8\text{O}_{27}$ (FW = 1676.80): C, 44.37, H, 3.45, N, 6.67%. Found: C, 45.05, H, 3.64, N, 6.57%.

Preparation of $\text{Mn}_{12}^{\text{II}}\text{Mn}_6^{\text{III}}$. A mixture of HCOOH (0.023 g, 0.50 mmol), ethylenediamine (0.03 g, 0.50 mmol), HIN (0.246 g, 2.00 mmol), NH_4VO_3 (0.005 g, 0.45 mmol), Gd_2O_3 (0.182 g, 0.50 mmol), $\text{Mn} \cdot (\text{CH}_3\text{COO})_2 \cdot 4\text{H}_2\text{O}$ (0.350 g, 2.00 mmol) and tetrahydrofuran (8.0 mL) was stirred at room temperature for 12 h. Then, this suspension was heated to 170 °C and kept for 10 days in a 25 mL Teflon-lined autoclave (Schemes 2 and S2†). After cooling for 48 h, a colourless block product was obtained. The product was washed with $\text{CH}_3\text{CH}_2\text{OH}$, and the yield of pure $\text{Mn}_{12}^{\text{II}}\text{Mn}_6^{\text{III}}$ was 38% (based on Mn). Anal. calcd for $\text{C}_{132}\text{H}_{123}\text{N}_{18}\text{O}_{73}\text{Mn}_{18}$ (FW = 4118.40): C, 38.32, H, 3.10, N, 6.05%. Found: C, 38.46, H, 3.00, N, 6.12%.

Scheme 2 Synthetic route of $\text{Mn}_{12}^{\text{II}}\text{Mn}_6^{\text{III}}$.Table 1 Summary of crystal data and structure results for compounds Mn_6^{II} and $\text{Mn}_{12}^{\text{II}}\text{Mn}_6^{\text{III}}$

Compound	$\text{Mn}_{12}^{\text{II}}\text{Mn}_6^{\text{III}}$	Mn_6^{II}
Empirical formula	$\text{C}_{132}\text{H}_{123}\text{Mn}_{18}\text{N}_{18}\text{O}_{73}$	$\text{C}_{62}\text{H}_{58}\text{Mn}_6\text{N}_8\text{O}_{27}$
Formula weight	4118.40	1676.80
Crystal system	Trigonal	Monoclinic
Space group	$P\bar{3}$	$C2/c$
<i>a</i> (Å)	24.293(8)	15.513(2)
<i>b</i> (Å)	24.293(8)	10.486(2)
<i>c</i> (Å)	9.537(5)	22.374(4)
α (deg)	90	90
β (deg)	90	107.311(3)
γ (deg)	120	90
Volume (Å ³)	4874(4)	3474.8(11)
<i>Z</i>	1	2
<i>D_c</i> (Mg m ⁻³)	1.403	1.603
μ (mm ⁻¹)	1.204	1.146
<i>F</i> (000)	2075	1704
Crystal size (mm ³)	0.160 × 0.130 × 0.130	0.150 × 0.100 × 0.100
Radiation type	Mo K α	Mo K α
2 θ range for data collection (°)	0.968–25.484	1.907–25.099
Limiting indices	−29 ≤ <i>h</i> ≤ 27 −28 ≤ <i>k</i> ≤ 29 −11 ≤ <i>l</i> ≤ 11	−17 ≤ <i>h</i> ≤ 18 −12 ≤ <i>k</i> ≤ 12 −26 ≤ <i>l</i> ≤ 26
Reflections collected	35 185	12 170
<i>R</i> _{int}	0.0763	0.0321
Data/restraints/parameters	6053/66/388	3100/19/252
Goodness-of-fit on <i>F</i> ²	1.081	1.037
Final <i>R</i> indices, <i>R</i> ₁ ^a , <i>wR</i> ₂ ^b	<i>R</i> ₁ = 0.0365 <i>wR</i> ₂ = 0.1071	<i>R</i> ₁ = 0.0268 <i>wR</i> ₂ = 0.0670
[<i>I</i> > 2 σ (<i>I</i>)]	<i>R</i> ₁ = 0.0459	<i>R</i> ₁ = 0.0308
<i>R</i> indices (all data)	<i>wR</i> ₂ = 0.1114	<i>wR</i> ₂ = 0.0692

$$^a R_1 = \frac{\sum ||F_o| - |F_c||}{\sum |F_o|}, \quad ^b wR_2 = \frac{\sum [w(F_o^2 - F_c^2)^2]}{\sum [w(F_o^2)^2]}^{1/2}.$$



Results and discussion

Synthesis

Developing a synthetic process for desired products with higher yields is much harder for the following reasons. The growth of target composition is sensitive for the initial reaction circumstances and conditions, such as the ratio of reactants, the type and ratio of solvents and the temperature.^{36,49–56} In this work, HCOOH, tetrahydrofuran, ethanediamine, $\text{Mn} \cdot (\text{CH}_3\text{COO})_2 \cdot 4\text{H}_2\text{O}$, and HIN were chosen as ideal reactants. In addition, we also tried out other organic solvents (ethyl alcohol, methyl alcohol, acetonitrile and *N,N*-dimethyl formamide) in the synthetic process, but no products could be synthesized. Ethanediamine was not observed in the final structure, but played an indispensable role in the construction of 3D Mn-clusters. Besides, HCOOH and ethanediamine must be measured at first. Interestingly, while adding NH_4VO_3 and Gd_2O_3 as the reactants, a beautiful structure with 18 Mn ions was obtained. We also optimized the reaction, and $\text{Mn}_{12}^{\text{II}}\text{Mn}_6^{\text{III}}$ was successfully synthesized in the presence of NH_4VO_3 and Gd_2O_3 . During the cooling process, the yield and morphology of products were unproductive for a cooling time of less than 48 h. Consequently, on cooling for over 48 h, two compounds were obtained with yields of 68% and 38%. In order to study the related properties regarding the two compounds, purification is an important step. The products were washed with $\text{CH}_3\text{CH}_2\text{OH}$ and then filtrated to obtain target products (Table 1).

Structure

Single-crystal X-ray analysis was performed, which made it clear that Mn_6^{II} and $\text{Mn}_{12}^{\text{II}}\text{Mn}_6^{\text{III}}$ crystallize in the monoclinic space

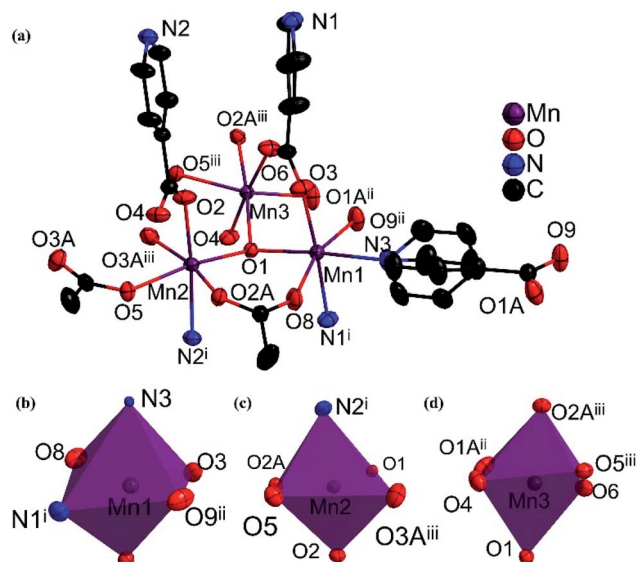


Fig. 2 The basic building block (a) and coordination models of Mn ions (b–d) in compound $\text{Mn}_{12}^{\text{II}}\text{Mn}_6^{\text{III}}$. [Symmetry code: (i) $x, y, 1 + z$; (ii) $-y, 1 + x - y, z$; (iii) $-1 + y, -1 - x + y, 2 - z$. H atoms have been deleted for clarity.]

group $C2/c$ and the trigonal space group $P\bar{3}$, respectively. As shown in Fig. 1a and b, the asymmetric unit of Mn_6^{II} contains six Mn^{II} ions, two CH_3COO^- groups, two HCOO^- groups and eight IN^- ligands, one free H_2O and two free tetrahydrofuran. Moreover, the asymmetric unit of $\text{Mn}_{12}^{\text{II}}\text{Mn}_6^{\text{III}}$ contains twelve Mn^{II} ions, six Mn^{III} ions (determined by XPS, Fig. 6), twelve CH_3COO^- , eighteen IN^- ligands, six $\mu_3\text{-O}^{2-}$ and 7.5 free water molecules (Fig. 2a). All Mn ions in Mn_6^{II} and $\text{Mn}_{12}^{\text{II}}\text{Mn}_6^{\text{III}}$ are hexacoordinated, displaying a near-octahedral geometry. As shown in Fig. S1,† Mn1 of Mn_6^{II} is coordinated to two N atoms (from two HIN) and four O atoms (from one HCOO^- and one CH_3COO^- and two IN^- groups); Mn2 of Mn_6^{II} is coordinated to six O atoms (from one HCOO^- and one CH_3COO^- and four IN^- groups). For $\text{Mn}_{12}^{\text{II}}\text{Mn}_6^{\text{III}}$ (Fig. 2b–d and S2†), Mn1 is coordinated to two N atoms (from two IN^- ligands) and four O atoms (from one $\mu_3\text{-O}^{2-}$ group, two IN^- ligands and one CH_3COO^- group); Mn2 is coordinated to one N atom (from one IN^- ligand) and five O atoms (from one $\mu_3\text{-O}^{2-}$ group), two Mn3 is coordinated to six O-donors (from one $\mu_3\text{-O}^{2-}$ group, three HIN ligands and two CH_3COO^- groups). The Mn–O bond lengths are between 2.131(3) and 2.277(2) Å as well as the Mn–N bond lengths are between 2.312(3) and 2.391(3) Å, which are approximate to the data obtained in the previously reported Mn-based compounds.^{3,31–34} However, in Mn_6^{II} and $\text{Mn}_{12}^{\text{II}}\text{Mn}_6^{\text{III}}$, the coordination modes of IN^- and CH_3COO^- ligands have only one mode, as indicated in Fig. S3,† which are both coordinated with three Mn ions.

As shown in Fig. 1f, the adjacent Mn_6^{II} units are linked by one CH_3COO^- , one HCOO^- and two IN^- ligands, forming a 1D chain structure. Besides, the three kinds of bridge-ligands are all parallel and reverse (Fig. 1c–f). The adjacent 1D chains are interconnected to form a 2D layer based on IN^- ligands only (Fig. 3a–e). The neighbouring 2D layers are further connected by

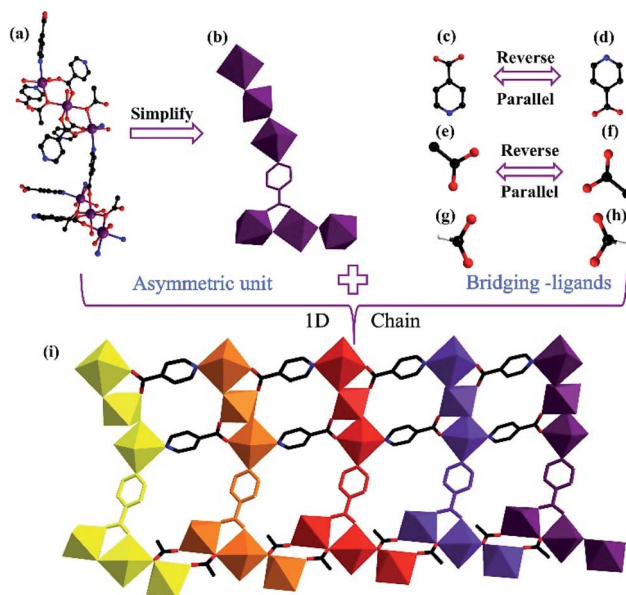


Fig. 1 The stick-ball pattern of Mn_6^{II} (a and b); the ball and stick of HIN (c and d); the ball and stick of CH_3COOH (e and f); the ball and stick of HCOOH (g and h); 1D chain-like structure unit in Mn_6^{II} (i). (O: red, N: blue, C: black, H: white, Mn: purple for (a)–(h)).



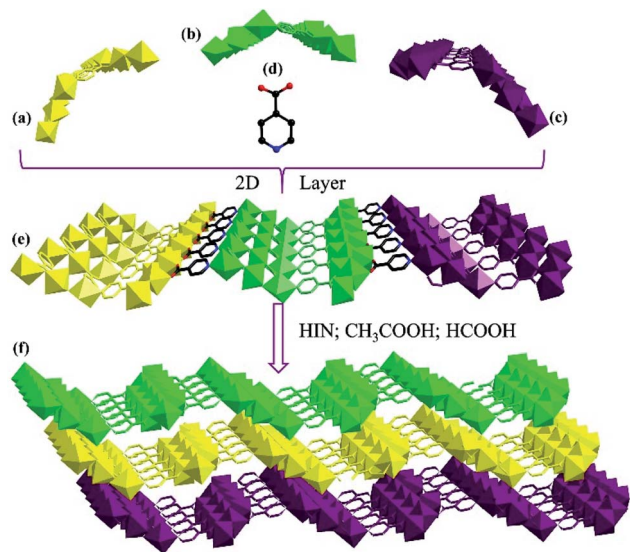


Fig. 3 The 1D chain structure of Mn_6^{II} (a–c); the ball and stick of HIN (d); the 2D-layer of Mn_6^{II} (e); the 3D structure of Mn_6^{II} (f).

IN^- , HCOO^- and CH_3COO^- ligands, forming a 3D structure (Fig. 3f).

As shown in the Fig. 4b and S8^\dagger $[\text{Mn}_2^{\text{II}}\text{Mn}^{\text{III}}(\mu_3\text{-O})(\text{CH}_3\text{-COO})_2]^{3+}$ unit (the first building unit; abbreviated as $\text{Mn}_2^{\text{II}}\text{Mn}^{\text{III}}$) consists of three Mn ions and two CH_3COO^- and one $\mu_3\text{-O}^{2-}$ group. As we can see in Fig. 4, the adjacent $\text{Mn}_2^{\text{II}}\text{Mn}^{\text{III}}$ units are lined by acetic acid, forming a $[\text{Mn}_{12}^{\text{II}}\text{Mn}_6^{\text{III}}(\mu_3\text{-O})_6(\text{CH}_3\text{COO})_{12}]^{18+}$ (the second building unit; abbreviated as the $\text{Mn}_{12}^{\text{II}}\text{Mn}_6^{\text{III}}$) unit. In addition, Mn2 and Mn3 from adjacent $\text{Mn}_2^{\text{II}}\text{Mn}^{\text{III}}$ units are linked by two CH_3COO^- groups to form a screwy wheel. As shown in Fig. 4d, 12 CH_3COO^- groups evenly distribute on both sides of the wheel. The wheel of $\text{Mn}_{12}^{\text{II}}\text{Mn}_6^{\text{III}}$ fragments are nearly planar (Fig. 4f). As indicated in Fig. 5b, the adjacent $\text{Mn}_{12}^{\text{II}}\text{Mn}_6^{\text{III}}$ are interconnected only by the IN^- ligands, forming a porous plane. Meanwhile, the HIN ligands act as bonds furtherly linked to adjacent $\text{Mn}_{12}^{\text{II}}\text{Mn}_6^{\text{III}}$ wheels, resulting in a 3D structure (Fig. 5c). Besides, adjacent IN^- ligands are all orderly arranged in the opposite direction (Fig. 5d).

XPS. In order to further prove the mixed valence of compound $\text{Mn}_{12}^{\text{II}}\text{Mn}_6^{\text{III}}$, an XPS measurement was carried out

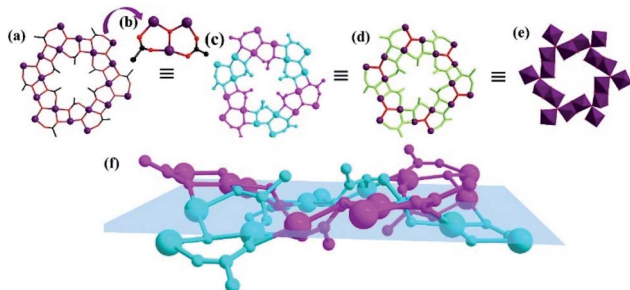


Fig. 4 The different expressional patterns of the $\text{Mn}_{12}^{\text{II}}\text{Mn}_6^{\text{III}}$ the coordination polymer (a) and (c–f); Ball and stick plot of $\text{Mn}_2^{\text{II}}\text{Mn}^{\text{III}}$ unit (b).

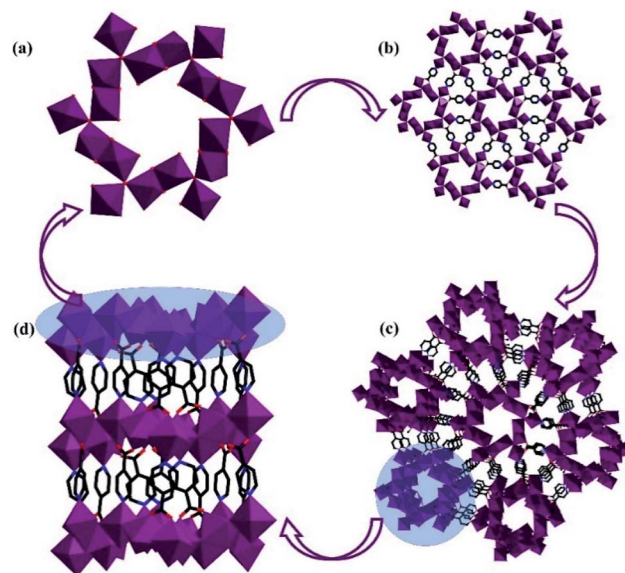


Fig. 5 Distribution of $\text{Mn}_{12}^{\text{II}}\text{Mn}_6^{\text{III}}$ (a); The 2D structure of compound $\text{Mn}_{12}^{\text{II}}\text{Mn}_6^{\text{III}}$ (b); 3D structure of the compound $\text{Mn}_{12}^{\text{II}}\text{Mn}_6^{\text{III}}$ (c); 1D channel in a three-dimensional structure of compound $\text{Mn}_{12}^{\text{II}}\text{Mn}_6^{\text{III}}$ (d).

(Fig. 6). By accurate fitting, peaks at 641.3 eV for $\text{Mn } 2p_{3/2}$ and 653.2 eV for $\text{Mn } 2p_{1/2}$ can be assigned to Mn^{II} ions.^{57–59} The characteristic peak at 645.8 eV proves the presence of Mn^{III} in $\text{Mn}_{12}^{\text{II}}\text{Mn}_6^{\text{III}}$.^{57–59} In addition, the XPS result suggests that the ratio ($\text{Mn}^{\text{II}} : \text{Mn}^{\text{III}}$) is 2 : 1, which is consistent with the result obtained from single-crystal X-ray diffractometry.

PXRD. PXRD of compounds Mn_6^{II} and $\text{Mn}_{12}^{\text{II}}\text{Mn}_6^{\text{III}}$ was studied at room temperature (Fig. S12 and S13[†]). The experimental patterns were basically similar to simulated curves, revealing that the structures of two compounds are similar to the results of SCXRD. The main peaks for $\text{Mn}_{12}^{\text{II}}\text{Mn}_6^{\text{III}}$ at 2θ of 4.20°, 7.28°, 8.40° and 9.26° can be indexed to the indices of crystal face of (0 0 2), (1 1 0), (−1 1 2) and (1 1 1) reflections, respectively. For Mn_6^{II} , main peaks at 2θ of 8.34°, 10.52°, and 11.90° can be

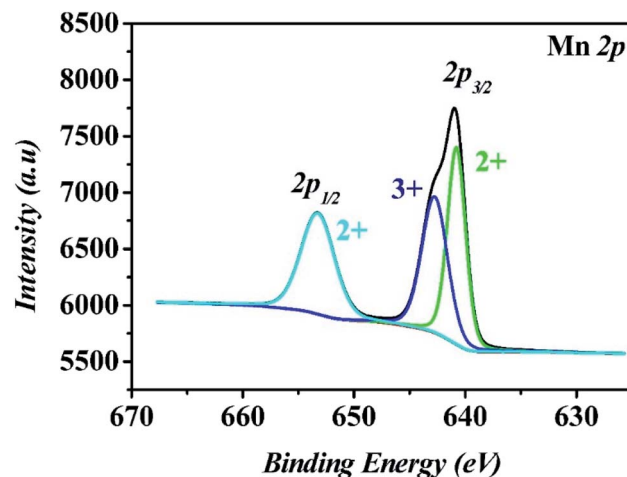


Fig. 6 The XPS for compound $\text{Mn}_{12}^{\text{II}}\text{Mn}_6^{\text{III}}$.



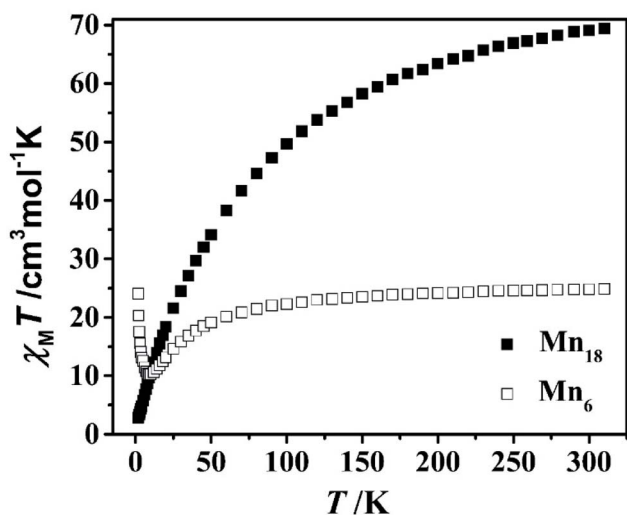


Fig. 7 Temperature-dependent magnetic susceptibilities for compound Mn_6^{II} and $\text{Mn}_{12}\text{Mn}_6^{\text{III}}$.

indexed to indices of crystal face of $(-1\ 2\ 0)$, $(0\ 2\ 0)$ and $(0\ 0\ 1)$ reflections, respectively. The result of PXRD indicates that compounds Mn_6^{II} and $\text{Mn}_{12}\text{Mn}_6^{\text{III}}$ are different Mn-based polymers, which are in agreement with SCXRD (as shown in Fig. S14[†]).

FT-IR spectra. The FT-IR spectra of Mn_6^{II} and $\text{Mn}_{12}\text{Mn}_6^{\text{III}}$ were studied at room temperature in the range of $\nu = 4000\text{--}400\text{ cm}^{-1}$ (Fig. S15 and S16[†]). The peaks at $3397\text{ (Mn}_6^{\text{II}})$ and $3382\text{ (Mn}_{12}\text{Mn}_6^{\text{III}})\text{ cm}^{-1}$ can be assigned to the stretching vibration of $-\text{OH}$ from H_2O or the air. The peaks at $1612\text{ (Mn}_6^{\text{II}})$ and $1604\text{ (Mn}_{12}\text{Mn}_6^{\text{III}})\text{ cm}^{-1}$ can be due to the presence of $-\text{COO}^-$. The characteristic peaks of the pyridine from the HIN are at $1550, 1400, 1342, 1218,$ and 1060 cm^{-1} for Mn_6^{II} , and $1550, 1440, 1214,$ and 1014 cm^{-1} for $\text{Mn}_{12}\text{Mn}_6^{\text{III}}$. The values are consistent with the related literature studies.^{3,31–36}

TG analysis. As shown in Fig. S17,[†] the TG curve of Mn_6^{II} was studied. The weight loss was 4.90% (theoretical value 4.27%) from 25 to 205 °C due to the loss of two free tetrahydrofuran and one H_2O . From 205 to 800 °C, the loss was 61.74% (theoretical value 61.80%) due to the collapse of the metal framework. The TGA analysis of product $\text{Mn}_{12}\text{Mn}_6^{\text{III}}$ was also carried out (Fig. S18[†]). The TGA diagram showed two main weight losses in the curve. The first step (25–200 °C) corresponds to the release of 7.5 free water. The observed weight loss of 3.9% is similar to the theoretical values (3.3%). Then, compound $\text{Mn}_{12}\text{Mn}_6^{\text{III}}$ lost a mass of 36.09% in the range of 200–800 °C. It can be attributed to the thermal decomposition of metal framework.

Magnetic properties. As displayed in Fig. 7, S19 and S20,[†] the $\chi_{\text{M}}T$ - T of compounds Mn_6^{II} and $\text{Mn}_{12}\text{Mn}_6^{\text{III}}$ was studied under 1000 Oe in the range of 1.8–300 K. At $T = 300\text{ K}$, the values of $\chi_{\text{M}}T$ were $24.87\text{ (Mn}_6^{\text{II}})$ and $69.60\text{ (Mn}_{12}\text{Mn}_6^{\text{III}})\text{ cm}^3\text{ K mol}^{-1}$, which were almost consistent with the calculated values $26.25\text{ (Mn}_6^{\text{II}})$ and $70.50\text{ (Mn}_{12}\text{Mn}_6^{\text{III}})\text{ cm}^3\text{ K mol}^{-1}$ (Mn^{II} ions, $S = 5/2$; Mn^{III} ions, $S = 2$).^{3,18} With the temperature cooling, $\chi_{\text{M}}T$ of compound Mn_6^{II} slowly decreased in the range of 90 K to 300 K. With cooling, $\chi_{\text{M}}T$ of compound Mn_6^{II} rapidly decreased to 10.23

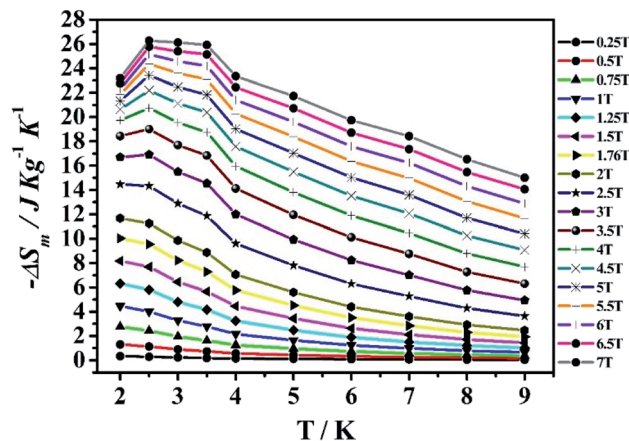


Fig. 8 Curves of $-\Delta S_{\text{m}}$ vs. T for compound Mn_6^{II} .

$\text{cm}^3\text{ K mol}^{-1}$ at 9 K. However, as the temperature decreased further, $\chi_{\text{M}}T$ abruptly rose to $24.08\text{ cm}^3\text{ K mol}^{-1}$ at 2.0 K. Besides, the χ_{M}^{-1} vs. T was fitted based on the Curie-Weiss law (from 1.8 to 300 K) with the result $C = 25.69\text{ cm}^3\text{ K mol}^{-1}$ and $\theta = -12.49\text{ K}$. The negative value of θ indicates that the antiferromagnetic behaviour may exist in Mn_6^{II} (Fig. S21[†]).¹⁸ For complex $\text{Mn}_{12}\text{Mn}_6^{\text{III}}$, the $\chi_{\text{M}}T$ decreased slowly along with the decrease in temperature, which was in good agreement with the antiferromagnetic behaviour.³ The plot of $1/\chi_{\text{M}}$ vs. T obeyed the Curie-Weiss law $\chi_{\text{M}}^{-1} = (T - \theta)/C$ with $C = 76.57\text{ cm}^3\text{ K mol}^{-1}$ and $\theta = -37.22\text{ K}$, and the negative product of θ further demonstrates antiferromagnetic interactions between adjacent Mn ions (Fig. S22[†]).²⁵

The M - H of compounds Mn_6^{II} and $\text{Mn}_{12}\text{Mn}_6^{\text{III}}$ was studied under $T = 1.8\text{--}10\text{ K}$ and $H = 0\text{--}7\text{ T}$ (Fig. S23 and S24[†]). Along with the increase in H , M (Mn_6^{II}) slowly increased, gradually saturated and reached $10.78\text{ N}\mu_{\text{B}}$ at 7 T. For $\text{Mn}_{12}\text{Mn}_6^{\text{III}}$, M slowly increased and reached $17.57\text{ N}\mu_{\text{B}}$ at 7 T with the increasing H .

The magnetization data of compounds Mn_6^{II} and $\text{Mn}_{12}\text{Mn}_6^{\text{III}}$ were analysed in the range of 2–9 K, based on the Maxwell relation in equation $\Delta S_{\text{m}}(T) = \int [\partial M(T, H)/\partial T]_{\text{H}} dH$.²⁵ The compound Mn_6^{II} is discussed first. The consequential maximum

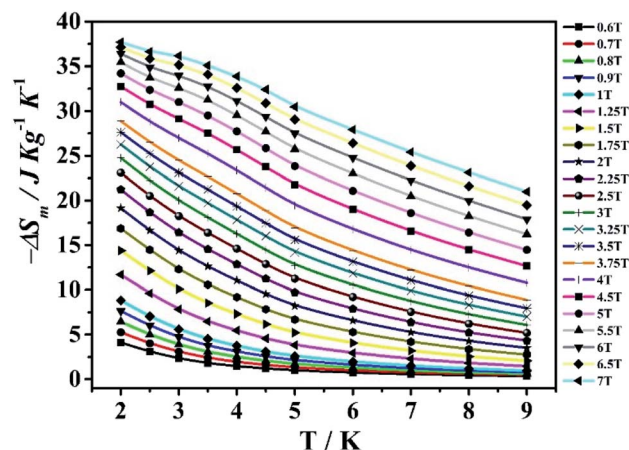


Fig. 9 Curves of $-\Delta S_{\text{m}}$ vs. T for compound $\text{Mn}_{12}\text{Mn}_6^{\text{III}}$.



Table 2 $-\Delta S_m^{\max}$ value for some Mn-base compounds under ΔH by the given temperature

Compound	$-\Delta S_m^{\max}$	ΔH (T)	Ref.
$[\text{Mn}(\text{glc})_2(\text{H}_2\text{O})_2]_n$	60.30	7.0	31
$\text{Mn}_{12}^{\text{II}}\text{Mn}_6^{\text{III}}$	37.69	7.0	This work
Mn_6^{II}	26.27	7.0	This work
$\text{Mn}_6^{\text{III}}\text{Mn}_8^{\text{II}}$	25.00	7.0	33
$\text{Fe}_{14}^{\text{III}}$	20.30	7.0	51
Mn_4^{II}	19.30	7.0	32
$\text{Mn}_6^{\text{III}}\text{Mn}_4^{\text{II}}$	17.00	7.0	33
Mn_2Gd	50.10	7.0	21
Mn_2Gd_2	37.90	9.0	52
Gd_{104}	46.9	7.0	53
Gd_{38}	37.9	7.0	54
Gd_{18}	25.9	5.0	55

value of $-\Delta S_m$ is $26.27 \text{ J kg}^{-1} \text{ K}^{-1}$ (Mn_6^{II}) at approximately 2.5 K and $\Delta H = 7 \text{ T}$ (Fig. 8), which was slightly smaller than the theoretical calculated value [$53.17 \text{ J kg}^{-1} \text{ K}^{-1}$, which was obtained on $R \ln(2S + 1)$].³³ The discrepancy could be due to the antiferromagnetic magnetic interaction among the metal ions.¹⁸ Besides, the maximum value of $-\Delta S_m$ was $37.69 \text{ J kg}^{-1} \text{ K}^{-1}$ ($\text{Mn}_{12}^{\text{II}}\text{Mn}_6^{\text{III}}$) at 2 K and $\Delta H = 7 \text{ T}$ (Fig. 9), which was slightly smaller than the theoretically calculated value [$62.71 \text{ J kg}^{-1} \text{ K}^{-1}$, which was gained by $R \ln(2S + 1)$].^{55,56} The discrepancy could be due to the antiferromagnetic magnetic interaction among metal ions.³³ The maximum values of $-\Delta S_m$ for compounds Mn_6^{II} and $\text{Mn}_{12}^{\text{II}}\text{Mn}_6^{\text{III}}$ are large in the pure 3d- or 4f-type and 3d-4f systems (Table 2). In addition, the $-\Delta S_m$ of $\text{Mn}_{12}^{\text{II}}\text{Mn}_6^{\text{III}}$ is largest in the pure Mn-type compounds, except for $[\text{Mn}(\text{glc})_2(\text{H}_2\text{O})_2]_n$.³¹

Conclusions

In summary, two 3D complexes (Mn_6^{II} and $\text{Mn}_{12}^{\text{II}}\text{Mn}_6^{\text{III}}$) were successfully synthesized based on solvothermal conditions. In terms of their synthesis, $\text{Mn}_{12}^{\text{II}}\text{Mn}_6^{\text{III}}$ was obtained by adding Gd_2O_3 and NH_4VO_3 in the synthesis of Mn_6^{II} , which is a valid synthesis process and may contribute to synthesizing numerous coordination polymers. Magnetic studies revealed that Mn_6^{II} and $\text{Mn}_{12}^{\text{II}}\text{Mn}_6^{\text{III}}$ are potential magnetic materials with $-\Delta S_m = 26.27$ and $37.69 \text{ J kg}^{-1} \text{ K}^{-1}$ respectively, which are much larger than the previously synthesized Mn-based coordination polymers. Moreover, the $-\Delta S_m$ value of $\text{Mn}_{12}^{\text{II}}\text{Mn}_6^{\text{III}}$ is almost the largest among pure Mn-type coordination polymers, making it a potential polymer in the MCE of pure 3d-type systems.

Conflicts of interest

There are no conflicts of interest to declare.

Acknowledgements

This work was supported by the Natural Science Foundation of China (Grant 21571103), Jiangsu Province (BK20191359), and the Major Natural Science Projects of the Jiangsu Higher Education Institution (Grant 16KJA150005).

Notes and references

- N. E. Chakov, W. Wernsdorfer, K. A. Abboud and G. Christou, *Inorg. Chem.*, 2004, **43**, 5919–5930.
- M. Murugesu, J. Raftery, W. Wernsdorfer, G. Christou and E. K. Brechin, *Inorg. Chem.*, 2004, **43**, 4203–4209.
- L. Zhou, B. Zhou, S. Cao, Z. Cui, B. Qin, W. Li, X. Zhang and J. Zhang, *Chem.–Eur. J.*, 2018, **24**, 19152–19155.
- S.-L. Li and Q. Xu, *Energy Environ. Sci.*, 2013, **6**, 1656–1683.
- S. Liu, Y. Deng and F. Xu, *Chem. Commun.*, 2020, **54**, 6066–6069.
- Y.-F. Li and Z.-P. Liu, *J. Am. Chem. Soc.*, 2018, **140**, 1783–1792.
- A. I. Nguyen, D. L. M. Suess, L. E. Darago, P. H. Oyala, D. S. Levine, M. S. Ziegler, R. D. Britt and T. D. Tilley, *J. Am. Chem. Soc.*, 2017, **139**, 5579–5587.
- T. Ghosh and G. Maayan, *Angew. Chem., Int. Ed.*, 2019, **58**, 2785–2790.
- A. J. Tasiopoulos, A. Vinslava, W. Wernsdorfer, K. A. Abboud and G. Christou, *Angew. Chem., Int. Ed.*, 2004, **43**, 2117–2121.
- U. S. Sadana, P. Sharma, N. C. Ortiz, D. Samal and N. Claassen, *J. Plant Nutr. Soil Sci.*, 2005, **168**, 581–589.
- J. Liang, Z. Liu, L. Qiu, Z. Hawash, L. Meng, Z. Wu, Y. Jiang, L. K. Ono and Y. Qi, *Adv. Energy Mater.*, 2018, **8**, 1800504–1800511.
- G. E. Kostakis, A. M. Ako and A. K. Powell, *Chem. Soc. Rev.*, 2010, **39**, 2238–2271.
- M. Manoli, S. Alexandrou, L. Pham, G. Lorusso, W. Wernsdorfer, M. Evangelisti, G. Christou and A. J. Tasiopoulos, *Angew. Chem., Int. Ed.*, 2016, **55**, 679–684.
- M. U. Anwar, L. N. Dawe, M. S. Alam and L. K. Thompson, *Inorg. Chem.*, 2012, **51**, 11241–11250.
- C. J. Milios, S. Piligkos and E. K. Brechin, *Dalton Trans.*, 2008, 1809–1817.
- T. Lis, *Acta Crystallogr., Sect. B: Struct. Crystallogr. Cryst. Chem.*, 1980, **36**, 2042–2046.
- A. M. Ako, I. J. Hewitt, V. Mereacre, R. Clrac, W. Wernsdorfer, C. E. Anson and A. K. Powell, *Angew. Chem., Int. Ed.*, 2006, **118**, 5048–5051.
- V. Mereacre, A. M. Ako, R. Clrac, W. Wernsdorfer, I. J. Hewitt, C. E. Anson and A. K. Powell, *Chem.–Eur. J.*, 2008, **14**, 3577–3584.
- B. Zhao, H.-L. Gao, X.-Y. Chen, P. Cheng, W. Shi, D.-Z. Liao, S.-P. Yan and Z.-H. Jiang, *Chem.–Eur. J.*, 2006, **12**, 149–158.
- T. C. Stamatatos, S. J. Teat, W. Wernsdorfer and G. Christou, *Angew. Chem., Int. Ed.*, 2009, **48**, 521–524.
- F.-S. Guo, Y.-C. Chen, J.-L. Liu, J.-D. Leng, Z.-S. Meng, P. Vrabel, M. Orendáč and M.-L. Tong, *Chem. Commun.*, 2012, **48**, 12219–12221.
- C. J. Milios, I. A. Gass, A. Vinslava, L. Budd, S. Parsons, W. Wernsdorfer, S. P. Perlepes, G. Christou and E. K. Brechin, *Inorg. Chem.*, 2007, **46**, 6215–6217.
- X. Ma, D. Zhao, L.-F. Lin, S.-J. Qin, W.-X. Zheng, Y.-J. Qi, X.-X. Li and S.-T. Zheng, *Inorg. Chem.*, 2016, **55**, 11311–11315.



- 24 M. Riaz, R. K. Gupta, H.-F. Su, Z. Jagličić, M. Kurmoo, C.-H. Tung, D. Sun and L.-S. Zheng, *Inorg. Chem.*, 2019, **58**, 14331–14337.
- 25 T. C. Stamatatos, V. Nastopoulos, A. J. Tasiopoulos, E. E. Moushi, W. Wernsdorfer, G. Christou and S. P. Perlepes, *Inorg. Chem.*, 2008, **47**, 10081–10089.
- 26 M. Soler, W. Wernsdorfer, K. Folting, M. Pink and G. Christou, *J. Am. Chem. Soc.*, 2004, **126**, 2156–2165.
- 27 E. E. Moushi, C. Lampropoulos, W. Wernsdorfer, V. Nastopoulos, G. Christou and A. J. Tasiopoulos, *J. Am. Chem. Soc.*, 2010, **132**, 16146–16155.
- 28 M. Manoli, R. Inglis, M. J. Manos, V. Nastopoulos, W. Wernsdorfer, E. K. Brechin and A. J. Tasiopoulos, *Angew. Chem., Int. Ed.*, 2011, **50**, 4441–4444.
- 29 A. Vinslava, A. J. Tasiopoulos, W. Wernsdorfer, K. A. Abboud and G. Christou, *Inorg. Chem.*, 2016, **55**, 3419–3430.
- 30 T. Shiga, H. Nojiri and H. Oshio, *Inorg. Chem.*, 2020, **59**, 4163–4166.
- 31 Y.-C. Chen, F.-S. Guo, J.-L. Liu, J.-D. Leng, P. Vrabel, M. Orendáč, J. Prokleška, V. Sechovský and M.-L. Tong, *Chem.–Eur. J.*, 2014, **20**, 3029–3035.
- 32 J.-P. Zhao, R. Zhao, Q. Yang, B.-W. Hu, F.-C. Liu and X.-H. Bu, *Dalton Trans.*, 2013, **42**, 14509–14515.
- 33 M. Manoli, A. Collins, S. Parsons, A. Candini, M. Evangelisti and E. K. Brechin, *J. Am. Chem. Soc.*, 2008, **130**, 11129–11139.
- 34 S. Nayak, M. Evangelisti, A. K. Powell and J. Reedijk, *Chem.–Eur. J.*, 2010, **16**, 12865–12872.
- 35 F. Shao, J.-J. Zhuang, M.-G. Chen, N. Wang, H.-Y. Shi, J.-P. Tong, G. Luo, J. Tao and L.-S. Zheng, *Dalton Trans.*, 2018, **47**, 16850–16854.
- 36 N.-F. Li, Q.-F. Lin, X.-M. Luo, J.-P. Cao and Y. Xu, *Inorg. Chem.*, 2019, **58**, 10883–10889.
- 37 Y. Yu, X. Pan, C. Cui, X. Luo, N. Li, H. Mei and Y. Xu, *Inorg. Chem.*, 2020, **59**, 5593–5599.
- 38 Q. Lin, J. Li, Y. Dong, G. Zhou, Y. Song and Y. Xu, *Dalton Trans.*, 2017, **46**, 9745–9749.
- 39 Q. Lin, Y. Zhang, W. Cheng, Y. Liu and Y. Xu, *Dalton Trans.*, 2017, **46**, 643–646.
- 40 J.-L. Liu, W.-Q. Lin, Y.-C. Chen, J.-D. Leng, F.-S. Guo and M.-L. Tong, *Inorg. Chem.*, 2013, **52**, 457–463.
- 41 J.-B. Peng, Q.-C. Zhang, X.-J. Kong, Y.-Z. Zheng, Y.-P. Ren, L.-S. Long, R.-B. Huang, L.-S. Zheng and Z. Zheng, *J. Am. Chem. Soc.*, 2012, **134**, 3314–3317.
- 42 J.-B. Peng, Q.-C. Zhang, X.-J. Kong, Y.-P. Ren, L.-S. Long, R.-B. Huang, L.-S. Zheng and Z. Zheng, *Angew. Chem., Int. Ed.*, 2011, **50**, 10649–10652.
- 43 Y.-Z. Zheng, M. Evangelisti and R. E. P. Winpenny, *Angew. Chem., Int. Ed.*, 2011, **123**, 3776–3779.
- 44 W.-P. Chen, J. Singleton, L. Qin, A. Camón, L. Engelhardt, F. Luis, R. E. P. Winpenny and Y.-Z. Zheng, *Nat. Commun.*, 2018, **9**, 1–6.
- 45 D. I. Alexandropoulos, L. Cunha-Silva, J. Tang and T. C. Stamatatos, *Dalton Trans.*, 2018, **47**, 11934–11941.
- 46 J.-D. Leng, J.-L. Liu and M.-L. Tong, *Chem. Commun.*, 2012, **48**, 5286–5288.
- 47 L. Sun, H. Chen, C. Ma and C. Chen, *Dalton Trans.*, 2015, **44**, 20964–20971.
- 48 L. Wang, R. Zhao, L.-Y. Xu, T. Liu, J.-P. Zhao, S.-M. Wang and F.-C. Liu, *CrystEngComm*, 2014, **16**, 2070–2077.
- 49 S. Jeong, X. Song, S. Jeong, M. Oh, X. Liu, D. Kim, D. Moon and M. S. Lah, *Inorg. Chem.*, 2011, **50**, 12133–12140.
- 50 X.-Y. Li, H.-F. Su, Q.-W. Li, R. Feng, H.-Y. Bai, H.-Y. Chen, J. Xu and X.-H. Bu, *Angew. Chem., Int. Ed.*, 2019, **58**, 10184–10188.
- 51 R. Shaw, R. H. Laye, L. F. Jones, D. M. Low, C. Talbot-Eeckelaers, Q. Wei, C. J. Milios, S. Teat, M. Helliwell, J. Raftery, M. Evangelisti, M. Affronte, D. Collison, E. K. Brechin and E. J. L. McInnes, *Inorg. Chem.*, 2007, **46**, 4968–4978.
- 52 T. Rajeshkumar, R. Jose, P. R. Remya and G. Rajaraman, *Inorg. Chem.*, 2019, **58**, 11927–11940.
- 53 J.-B. Peng, X.-J. Kong, Q.-C. Zhang, M. Orendáč, J. Prokleška, Y.-P. Ren, L.-S. Long, Z. Zheng and L.-S. Zheng, *J. Am. Chem. Soc.*, 2014, **136**, 17938–17941.
- 54 F.-S. Guo, Y.-C. Chen, L.-L. Mao, W.-Q. Lin, J.-D. Leng, R. Tarasenko, M. Orendáč, J. Prokleška, V. Sechovský and M.-L. Tong, *Chem.–Eur. J.*, 2013, **19**, 14876–14885.
- 55 K. Wang, Z.-L. Chen, H.-H. Zou, K. Hu, H.-Y. Li, Z. Zhang, W.-Y. Sun and F.-P. Liang, *Chem. Commun.*, 2016, **52**, 8297–8300.
- 56 X.-M. Luo, Z.-B. Hu, Q.-f. Lin, W. Cheng, J.-P. Cao, C.-H. Cui, H. Mei, Y. Song and Y. Xu, *J. Am. Chem. Soc.*, 2018, **140**, 11219–11222.
- 57 S. L. Xiong, J. S. Chen, X. W. Lou and H. C. Zeng, *Adv. Funct. Mater.*, 2012, **22**, 861–871.
- 58 X. Li, Y. Zhu, X. Zhang, J. Liang and Y. Qian, *RSC Adv.*, 2013, **3**, 10001–10006.
- 59 B. J. Tan, K. J. Klabunde and P. M. A. Sherwood, *J. Am. Chem. Soc.*, 1991, **113**, 855–861.

